The Astrophysical Journal, 876:21 (9pp), 2019 May 1 https://doi.org/10.3847/1538-4357/ab11c2

The Inflow and Outflow Rate Evolution of Local Milky Way–mass Star-forming Galaxies since $z = 1.3$

Zhizheng Pan[1,2], Yingjie Peng[3], Xianzhong Zheng[1,2], Jing Wang[3], and Xu Kong[2,4]
[1] Purple Mountain Observatory, Chinese Academy of Sciences, 8 Yuan Hua Road, Nanjing, Jiangsu 210008, People's Republic of China; panzz@pmo.ac.cn
[2] School of Astronomy and Space Sciences, University of Science and Technology of China, Hefei, 230026, People's Republic of China; xzzheng@pmo.ac.cn
[3] Kavli Institute for Astronomy and Astrophysics, Peking University, Yi He Yuan Lu 5, Hai Dian District, Beijing 100871, People's Republic of China
[4] CAS Key Laboratory for Research in Galaxies and Cosmology, Department of Astronomy, University of Science and Technology of China, Hefei, Anhui 230026, People's Republic of China; xkong@ustc.edu.cn
Received 2018 September 25; revised 2019 March 18; accepted 2019 March 19; published 2019 April 29

Abstract

We study the gas inflow rate ($\zeta_{\rm inflow}$) and outflow rate ($\zeta_{\rm outflow}$) evolution of local Milky Way–mass star-forming galaxies (SFGs) since $z = 1.3$. The stellar mass growth history of Milky Way–mass progenitor SFGs is inferred from the evolution of the star formation rate (SFR)−stellar mass (M_*) relation, and the gas mass ($M_{\rm gas}$) is derived using the recently established gas-scaling relations. With the $M_* + M_{\rm gas}$ growth curve, the net inflow rate κ is quantified at each cosmic epoch. At $z \sim 1.3$, κ is comparable with the SFR, whereas it rapidly decreases to $\sim$0.15 $\times$ SFR at $z = 0$. We then constrain the average outflow rate $\zeta_{\rm outflow}$ of progenitor galaxies by modeling the evolution of their gas-phase metallicity. The best-fit $\zeta_{\rm outflow}$ is found to be (0.5–0.8) $\times$ SFR. Combining κ and $\zeta_{\rm outflow}$, we finally investigate the evolution of $\zeta_{\rm inflow}$ since $z = 1.3$. We find that $\zeta_{\rm inflow}$ rapidly decreases by $\sim$80% from $z = 1.3$ to $z = 0.5$. At $z < 0.5$, $\zeta_{\rm inflow}$ continuously decreases but with a much lower decreasing rate. Implications of these findings on galaxy evolution are discussed.

Key words: galaxies: evolution

1. Introduction

In the current galaxy formation paradigm, gas flows into and out of galaxies are key ingredients for driving galaxy evolution (Bouché et al. 2010; Davé et al. 2011, 2012; Lilly et al. 2013; Peng & Maiolino 2014). Observational studies suggest that gas inflows are required for star-forming galaxies (SFGs), as their gas depletion timescale is significantly shorter than that required to build up their stellar mass in both the low-redshift and high-redshift universe (Larson et al. 1980; Genzel et al. 2015; Tacconi et al. 2018). As an important feedback mechanism, gas outflows driven by star formation or an active galactic nucleus (AGN) can blow the metal-enriched gas out of a galaxy, regulating its chemical enrichment and star formation (Peeples & Shankar 2011; Hopkins et al. 2012; Cicone et al. 2014; Geach et al. 2014).

Theoretical works have predicted that gas inflows are achieved in two different modes, which are termed as the "cold mode" and the "hot mode" accretion (e.g., Kereš et al. 2005; Dekel & Birnboim 2006). In low-mass halos and high-redshift universe, gas is acquired primarily through the cold mode accretion, by which cold gas flows can directly feed galaxies through cosmic filaments (Kereš et al. 2005; Dekel et al. 2009a, 2009b; van de Voort et al. 2011). When a galaxy's dark matter halo grows massive enough to support a stable shock, the infalling gas is first shock-heated to near the viral temperature ($T \sim 10^6$ K), then radiatively cools and settles into galaxies in a quasi-spherical manner. The transition of these two accretion modes is expected to occur near the critical halo mass, $M_{\rm c} \sim 10^{12}\,M_\odot$ (Dekel & Birnboim 2006). To justify this, it is important to investigate the behavior of gas accretion when a galaxy evolves across $M_{\rm c}$. Simulations suggest that the gas accretion behavior indeed changes near $M_{\rm c}$ (Stewart et al. 2011), but observational confirmation of this is still lacking.

Observationally, gas flow signatures have been unambiguously detected in the high-quality spectra of SFGs (e.g., Heckman et al. 1990; Sato et al. 2009; Weiner et al. 2009; Genzel et al. 2014a; Rubin et al. 2014; Cicone et al. 2016). Nevertheless, the detailed properties of gas flows are still difficult to quantify directly. This is because gas flows can occur in multi-phase, and the global gas flow rates depend on the 3D motions and densities of the gas. Indirect methods are thus useful in studying gas flows. For example, early attempts have tried to set constraints on gas flows by modeling the chemical evolution of SFGs to match the observed mass–metallicity relation (Finlator & Davé 2008; Spitoni et al. 2010, 2017; Lilly et al. 2013; Yabe et al. 2015).

The assembly history of Milky Way–mass ($M_{\rm MW} \sim 5 \times 10^{10}\,M_\odot$, see McMillan 2017) galaxies has recently attracted much attentions, since galaxies near $M_{\rm MW}$ appear quite typical and dominate the stellar mass budget in the local universe (van Dokkum et al. 2013). Several works have tried to trace the evolution of star formation and morphology of $M_{\rm MW}$ progenitor galaxies back to $z = 1$–2 (Patel et al. 2013; van Dokkum et al. 2013; Papovich et al. 2015). In this paper, we aim to study the gas inflow and outflow history of local $M_{\rm MW}$ SFGs using an indirect approach. In Section 2, we first use the technique developed by Leitner & Kravtsov (2011) to select $M_{\rm MW}$ progenitor SFGs up to $z = 1.3$. In Section 3, we infer the molecular gas mass ($M_{\rm H2}$) of progenitor galaxies using the scaling relation recently established by Tacconi et al. (2018), and the atomic gas mass ($M_{\rm H\,I}$) is inferred using the $M_{\rm H\,I}$–M_* relation established at $z = 0$. In Section 4, we quantify the net inflow rate evolution of progenitor galaxies with the $M_* + M_{\rm gas}$ growth curve. In Section 5, we use an analytical chemical evolution model to set constraints on the outflow rate of progenitor galaxies. With the derived net inflow rate and outflow rate, we can investigate the gas inflow history of the local $M_{\rm MW}$ SFGs. In Section 6, we discuss the implication of our results. Finally, we summarize our findings in Section 7. Throughout this paper, we adopt a concordance

ΛCDM cosmology with $\Omega_m = 0.3$, $\Omega_\Lambda = 0.7$, $H_0 = 70\,\mathrm{km\,s^{-1}\,Mpc^{-1}}$ and a Chabrier (2003) initial mass function (IMF). All reported gas masses in this work include a correction of 1.36 to account for helium.

2. Stellar Mass Growth History of Progenitor Galaxies

We use the method developed by Leitner & Kravtsov (2011), namely the Main Sequence Integration (MSI) approach, to select progenitors of SFGs that with the final stellar mass of $\log(M_*/M_\odot) = 10.7$. The philosophy of this method is simple: if SFGs assemble most of their stellar mass from in situ star formation, then for a given redshift interval, the new stellar mass added to the existing mass is computable based on the location of the galaxy on the SFR–M_* plane and mass loss from stellar evolution modeling. For local $M_{\rm MW}$ SFGs, this method should be valid as galaxies with stellar masses near or below $M_{\rm MW}$ assemble their mass mainly from in situ star formation, not from mergers (Qu et al. 2017; Behroozi et al. 2018). From the observational perspective, the assumption that local $M_{\rm MW}$ SFGs are always star-forming in the past is supported by the stellar population constituents of the Milky Way disk (Haywood et al. 2016). Details of the MSI approach can be found in Leitner & Kravtsov (2011).

The SFR–M_* relation we used is from the work of Speagle et al. (2014), in which the evolution of the SFR–M_* relation at $z = [0, 6]$ is systematically investigated based on the compiled data from 25 studies. At each cosmic epoch, the SFR–M_* relation can be characterized by

$$\log \mathrm{SFR}(M_*, t) = (0.84 - 0.026 \times t)\log M_* - (6.51 - 0.11 \times t), \quad (1)$$

where t is the age of the universe in Gyr. Note that at a given t, the SFR–M_* relation is parameterized by a single power law. This may be problematic since the SFR–M_* relation appears having different power-law indices in the low- and high-mass regimes, as reported in some recent studies (Whitaker et al. 2014; Lee et al. 2015; Schreiber et al. 2015; Tomczak et al. 2016). To investigate whether Equation (1) is a good description of the star formation main sequence, we have compared the SFR–M_* relation of Speagle et al. (2014) with those of Whitaker et al. (2014) and Tomczak et al. (2016). At the same cosmic epoch, we find that these works report a remarkably consistent SFR–M_* relation at $\log(M_*/M_\odot) = [10.0,11.0]$, with a typical discrepancy of $\Delta \log \mathrm{SFR} < 0.05$ dex at fixed M_*. Since, in this work, we only trace progenitor galaxies back to $z = 1.3$ where they have a stellar mass of $\log(M_*/M_\odot) = 10.0$, the stellar mass growth history inferred from Equation (1) should be robust.

In Figure 1, we show the mass growth history of progenitor galaxies. To account for the uncertainty of the evolution of the main sequence, we arbitrarily allow a ±0.1 dex variation in the star formation rate ($\Delta \log(\mathrm{SFR}) = 0.1$). The resulting uncertainty in the stellar mass growth history ($\Delta \log M_*$) is shown in the hatched region. When increasing $\Delta \log(\mathrm{SFR}) = 0.1$ to $\Delta \log(\mathrm{SFR}) = 0.3$, $\Delta \log M_*$ increases by a factor of 5 and ∼1.5 at $z \sim 1.3$ and $z \sim 0.5$, respectively. For comparison, we also show the mass growth history of Milky Way–mass galaxies presented by van Dokkum et al. (2013), who select progenitor galaxies with a constant cumulative comoving number density of $\rho_c = 1.1 \times 10^{-3}\,\mathrm{Mpc^{-3}}$. It is clear from Figure 1 that the number density selection method is always biased to select more massive galaxies. This is because van Dokkum et al. (2013) also select the progenitors of quiescent Milky Way–mass galaxies. With a same final mass, it is natural that the quiescent ones will always assemble much earlier than the star-forming ones. It is worthy to note that the inferred mass growth history of progenitor galaxies becomes increasingly uncertain toward high redshifts. Given this, in the following we only focus on the evolution of progenitor galaxies at $z < 1.3$.

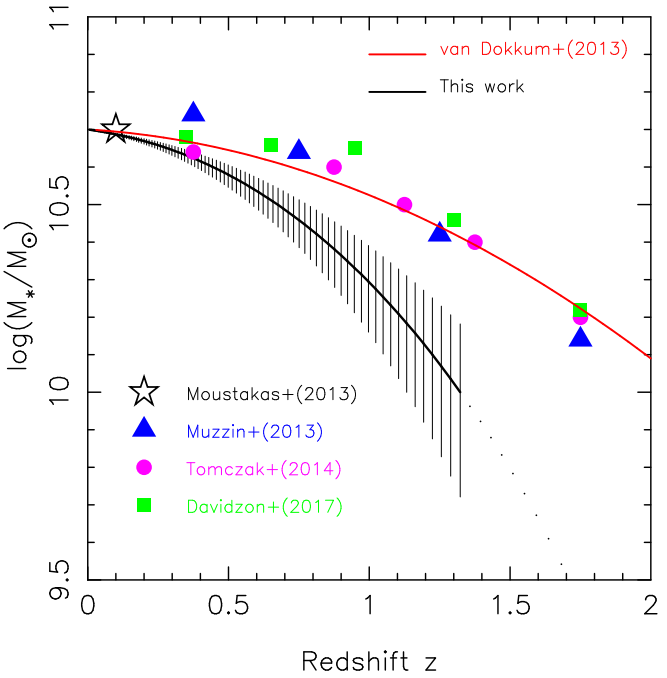

Figure 1. Black solid curve shows the stellar mass growth history of a SFG that with $\log(M_*/M_\odot) = 10.7$ at $z = 0$. Considering the different main-sequence parameterizations of different works, we include a ±0.1 dex variation in the main sequence parameterized in Equation (1). The resulting uncertainty in the stellar mass growth history is shown in the hatched region. The inferred stellar mass growth history becomes increasingly uncertain toward high redshift. We also show the mass growth history given by van Dokkum et al. (2013, red curve), who select the Milky Way–mass progenitor galaxies with a constant cumulative comoving number density of $\rho_c = 1.1 \times 10^{-3}\,\mathrm{Mpc^{-3}}$. The large symbols indicate the stellar mass at which the cumulative comoving density reaches $\rho_c = 1.1 \times 10^{-3}\,\mathrm{Mpc^{-3}}$, which are drawn from some recently published stellar mass functions.

3. The Determination of Cold Gas Mass $M_{\rm gas}$

The cold gas component of a galaxy consists of molecular and atomic hydrogen (H_2 and H I). Thanks to the increasing galaxy sample collected by recent molecular gas surveys (e.g., Daddi et al. 2010; Tacconi et al. 2010, 2013; Combes et al. 2011; Saintonge et al. 2011, 2017), scaling relations between molecular gas mass ($M_{\rm H_2}$), redshifts, and star formation rates for SFGs are now established. The seminal work of Genzel et al. (2015) compiled data from a number of molecular gas surveys at $z = [0, 3]$ to establish scaling relations between $\tau_{\rm H_2}$ (the H_2 depletion timescale, defined as $\tau_{\rm H_2} = M_{\rm H_2}/\mathrm{SFR}$), M_*, the SFR, and redshift z, enabling the determination of $M_{\rm H_2}$ for SFGs to an accuracy of ±0.2 dex. Recently, Tacconi et al. (2018) updated and improved the scaling relations of Genzel et al. (2015) using a larger sample spanning $z = [0, 4]$. With the new scaling relations, it is possible to determine $\tau_{\rm H_2}$ (or $M_{\rm H_2}$) to an accuracy of ±0.1 dex or better for sample averages. For SFGs that lie on the ridge line of the SFR–M_* relation of

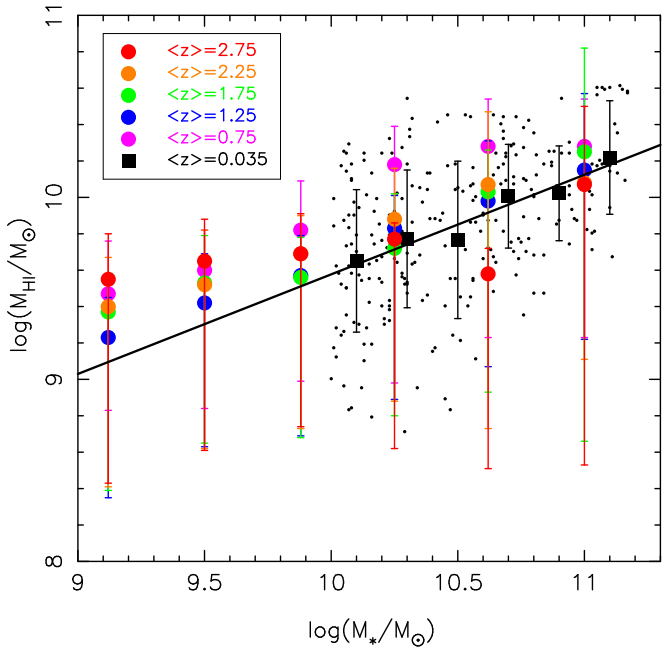

Figure 2. Log ($M_{\rm H\,I}$)–log(M_*) relation of SFGs. Small black symbols are SFGs with direct H I measurements from the GASS survey, with definite H I detection and near-ultraviolet (NUV) $-r < 4.0$. Large color symbols are from Popping et al. (2015). The running median of the GASS galaxies are shown in black squares. The black solid line is the linear fit of the GASS sample. Error bars indicate the 1σ scatter.

Speagle et al. (2014), the dependence of $\tau_{\rm H_2}$ on redshift can be characterized by

$$\log(\tau_{\rm H2}) = 0.09 - 0.62\log(1+z) \quad {\rm Gyr}, \tag{2}$$

where z is the redshift. As shown in Tacconi et al. (2018), $\tau_{\rm H_2}$ shows no clear dependence on M_*, at least at $\log(M_*/M_\odot) > 10.0$. Therefore, we can infer the $M_{\rm H_2}$ of progenitor galaxies at any cosmic epoch with

$$\log(M_{\rm H_2}/M_\odot) = \log({\rm SFR}) + \log(\tau_{\rm H_2}). \tag{3}$$

Direct determination of the H I mass of galaxies ($M_{\rm H\,I}$) at $z > 0.3$ is currently not realistic. Recently, Popping et al. (2015) used an indirect technique to infer the evolution of the cold gas of SFGs from $z = 3$ to $z = 0.5$, finding that at fixed M_*, the $M_{\rm H\,I}$ of SFGs shows no redshift dependence. In the local universe, deep H I surveys such as the GALEX Arecibo SDSS Survey (GASS; Catinella et al. 2010, 2013) have compiled a representative galaxy sample to enable a direct investigation of the H I mass for typical massive SFGs. In Figure 2, we compare the $M_{\rm H\,I}$–M_* relations of Popping et al. (2015) with that of the GASS sample. For the GASS galaxies, only those with both clear star formation (NUV $- r < 4.0$) and H I detection are selected. It can be seen that these two data sets show very good consistency. For the GASS galaxies, we fit the $M_{\rm H\,I}$–M_* relation with

$$\log(M_{\rm H\,I}/M_\odot) = 0.55\log(M_*/M_\odot) + 4.11, \tag{4}$$

as shown in the black solid line in Figure 2.

In what follows, we assume that the $M_{\rm H\,I}$–M_* relation has no evolution at $z = [0, 1.3]$, and $M_{\rm gas}$ is referred as $M_{\rm gas} = M_{\rm H\,I} + M_{\rm H_2}$.

4. The Growth History of $M_* + M_{gas}$ and the Inferred Net Gas Inflow Rate

In the left panel of Figure 3, we show the growth curves of M_* and $M_* + M_{\rm gas}$ for progenitor galaxies. It can be seen that $M_* + M_{\rm gas}$ grows much faster than M_*. At $z = 0.5$, $M_* + M_{\rm gas}$ has assembled ~90% of its final mass, whereas only ~75% of the final stellar mass is assembled. Since M_* contributes to the majority of the total baryonic budget at most epochs ($z < 1$), the uncertainty of the $M_* + M_{\rm gas}$ growth curve is thus dominated by the uncertainty in the M_* determination, i.e., the star formation history.

With the growth curve of $M_* + M_{\rm gas}$ in hand, we can quantify the evolution of net inflow rate κ. In a specific time interval of $\Delta t = t - t_0$, the net inflow mass is

$$M_{\rm net} = M_{\rm inflow} - M_{\rm outflow}, \tag{5}$$

where $M_{\rm inflow}$ and $M_{\rm outflow}$ are the inflow and outflow mass during Δt, respectively. From mass conservation, it is straightforward that

$$(M_* + M_{\rm gas})_t = (M_* + M_{\rm gas})_{t0} + M_{\rm net}. \tag{6}$$

Then the net inflow rate κ can be written as

$$\kappa = \frac{M_{\rm net}}{\Delta t} = \frac{(M_* + M_{\rm gas})_t - (M_* + M_{\rm gas})_{t0}}{\Delta t}. \tag{7}$$

In a more standard form, the brackets of Equations (6) and (7) should include the mass of ionized gas and dust. However, in SFGs the mass of dust and ionized gas are both around two orders of magnitude lower than the mass of cold gas (Wolfire et al. 2003; Rémy-Ruyer et al. 2014). Therefore, ignoring these two components should be safe. In the right panel of Figure 3, we show the SFR and κ as functions of look-back time $t_{\rm lb}$. Some interesting information can be read from this panel. First, the SFR reaches the peak value later than κ. This is comprehensible since to trigger star formation, the accreted gas needs to be further condensed. Second, the SFR declines by a factor $\sim \times 10$ from $z = 1.3$ to $z = 0$, while at the same period κ declines by a factor of $\sim \times 50$. At $z \sim 0$, such a low net inflow rate ($\kappa \sim 0.15 \times$ SFR) is far from sufficient to sustain the observed SFR. The fuel required for star formation in the present-day $M_{\rm MW}$ SFGs is thus mostly from internal sources, such as the recycled gas (Leitner & Kravtsov 2011) and the remaining gas reservoir.

We note that GASS is a very deep H I survey, and the $M_{\rm H\,I}$–M_* relation of GASS may be biased to gas-poor SFGs. To test how the $M_{\rm H\,I}$–M_* relation impacts on our result, we have also applied the $M_{\rm H\,I}$–M_* relation of the Arecibo Legacy Fast ALFA sample (ALFALFA; Giovanelli et al. 2005) in our analysis. The ALFALFA survey is biased to H I -rich galaxies, as demonstrated in Huang et al. (2012). At $\log(M_*/M_\odot) > 10.0$, the ALFALFA galaxies are systematically around 0.2 dex more rich in H I mass than the GASS galaxies. When applying the $M_{\rm H\,I}$–M_* relation of ALFALFA, we found that the results are not changed. This is because $M_{\rm H\,I}$ only contributes to the minority of the baryonic mass budget (<30%) at $\log M_*/M_\odot > 10.0$ even when the $M_{\rm H\,I}$–M_* relation of ALFALFA is applied, thus having little impact on the $M_* + M_{\rm gas}$ growth curve. We thus conclude that a slight modification on the $M_{\rm H\,I}$–M_* relation will not have a significant impact on our results.

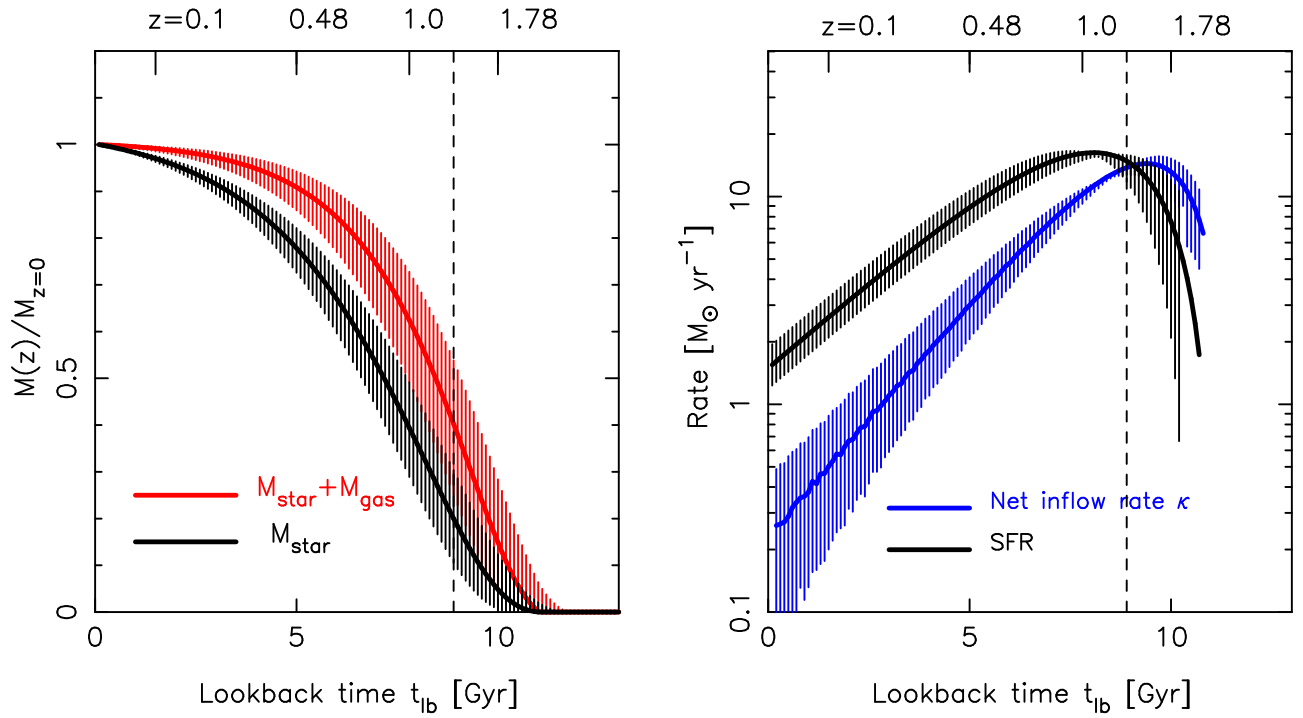

Figure 3. Left: growth curves of M_* (black line) and $M_* + M_{\rm gas}$ (red line). The uncertainties are calculated allowing variations of ± 0.1 dex in the SFR, ± 0.1 dex in $M_{\rm H_2}$ and ± 0.2 dex in $M_{\rm H\,I}$, respectively. The dashed line indicates $z = 1.3$, beyond which the growth history of galaxies becomes very uncertain. With the $M_* + M_{\rm gas}$ growth curve, we can quantify net gas inflow rate κ for progenitor galaxies, as shown in Equation (7). Right: the evolution of the SFR (black line) and κ (blue line).

5. Constraining the Inflow and Outflow Rates

The gas-phase metallicity, $Z_{\rm gas}$, can provide valuable insights in constraining the outflow properties of galaxies (Finlator & Davé 2008; Lilly et al. 2013; Belfiore et al. 2016). In this section, we will compare the observed $Z_{\rm gas}$ evolution of progenitor galaxies with that from a chemical evolution toy model to set constraints on the outflow rate $\zeta_{\rm outflow}$. Once $\zeta_{\rm outflow}$ is known, then we can investigate the inflow rate of these galaxies as the net inflow rate κ has been determined.

For a galaxy that with a known M_* growth history, its $Z_{\rm gas}$ at different redshifts can be inferred by utilizing the observed M_*–$Z_{\rm gas}$ relation (MZR)(Maiolino et al. 2008; Zahid et al. 2013, 2014). However, deriving the $Z_{\rm gas}$ evolution in this way may suffer large uncertainties, since different authors derive the MZRs using different sample section criteria and metallicity calibrations. To derive $Z_{\rm gas}$ in a consistent way across the probed redshift range, we infer $Z_{\rm gas}$ utilizing the tight correlation between $Z_{\rm gas}$, M_*, and the SFR established at $z = 0$. Based on the large $z = 0$ SFG sample, Mannucci et al. (2010) found that there exists a tight correlation among these three quantities, which can be expressed as

$$12 + \log({\rm O/H}) = 8.90 + 0.39x - 0.20x^2 - 0.077x^3 + 0.064x^4, \quad (8)$$

where $x = \log(M_*) - 0.32\log({\rm SFR}) - 10$.

Mannucci et al. (2010) found that galaxies at $z < 2.5$ appear all follow this relation, which they termed as the fundamental metallicity relation (FMR). There have been many recent studies investigating whether this M_*–SFR–$Z_{\rm gas}$ relation evolves from high-z to low-z. At $z < 1.5$, the FMR seems do not evolve (Cresci et al. 2012; Yabe et al. 2014). At higher redshifts, some studies report a same FMR as that established at $z = 0$ (Henry et al. 2013; Maier et al. 2014), while some studies reported a possible redshift evolution in this relation (Salim et al. 2015; Sanders et al. 2015, 2018). Since this work focuses on the evolution of $M_{\rm MW}$ progenitor SFGs at $z < 1.3$, we assume that the FMR does not evolve during this epoch. Inserting the M_* and SFR of progenitor galaxies into Equation (8), we derive the $Z_{\rm gas}$ evolution, as shown in the red symbols of Figure 4.

By making some simple assumptions, the evolution of $Z_{\rm gas}$ can be derived analytically. By definition, $Z_{\rm gas} = M_{\rm Z,gas}/M_{\rm gas}$, where $M_{\rm Z,gas}$ is the mass of metals in the gas reservoir. For a given SFG, $M_{\rm Z,gas}$ can increase by the input of metals from star formation and metal-enriched inflows, or it can decrease by gas outflows and the lockup of metals into long-lived stars. Assuming the inflow gas has metallicity Z_0 and the metal produced by star formation is $y \times$ SFR (where y is the nucleosynthetic yield per stellar population), from the mass conservation of metals, the change of $M_{\rm Z,gas}$ per unit time, $dM_{\rm Z,gas}/dt$, can be written as

$$\frac{dM_{\rm Z,gas}}{dt} = (y \cdot {\rm SFR} + Z_0 \cdot \zeta_{\rm inflow}) - Z_{\rm gas} \cdot \zeta_{\rm outflow} - Z_{\rm gas}(1 - R) \cdot {\rm SFR}, \quad (9)$$

where $\zeta_{\rm inflow}$ and $\zeta_{\rm outflow}$ are gas inflow and outflow rate, and R is the return mass fraction (defined as $R =$ mass loss rate/SFR), respectively. The last term represents the metal that locked in long-live stars. Following the definition of $Z_{\rm gas}$, then

$$\frac{dZ_{\rm gas}}{dt} = y\frac{\rm SFR}{M_{\rm gas}} - (Z_{\rm gas} - Z_0)\frac{\zeta_{\rm inflow}}{M_{\rm gas}}. \quad (10)$$

Assuming that $\zeta_{\rm inflow}$, $M_{\rm gas}$, y, and the SFR are all constant or only change slowly during the time interval $\Delta t = t - t_0$, then

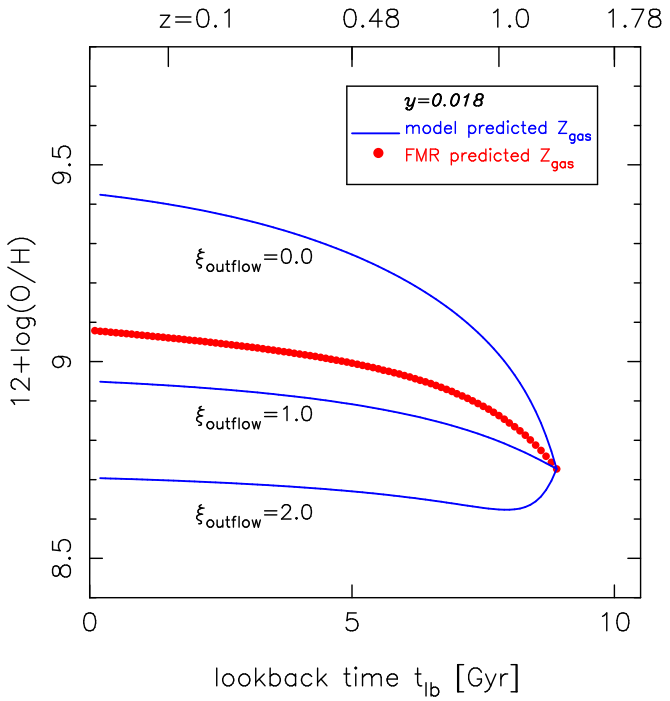

Figure 4. For illustration, we compare the FMR predicted $Z_{\rm gas}$ evolution from $z = 1.3$ to $z = 0$ for progenitor galaxies (red symbols) with three examples from our analytical chemical evolution model (blue lines). In each model, the nucleosynthetic yield is fixed to $y = 0.018$.

the solution of Equation (10) is

$$Z_{\rm gas}(t) = Z_0 + y\frac{\rm SFR}{\zeta_{\rm inflow}} + \left[Z_{\rm gas}(t_0) - Z_0 - y\frac{\rm SFR}{\zeta_{\rm inflow}}\right] \times e^{-\frac{\zeta_{\rm inflow}}{M_{\rm gas}}(t-t_0)}, \quad (11)$$

as given by Peng & Maiolino (2014).

When presenting the outflow rate $\zeta_{\rm inflow}$ in units of the SFR:

$$\zeta_{\rm inflow} = \xi_{\rm outflow} \cdot {\rm SFR}, \quad (12)$$

where $\zeta_{\rm inflow}$ can be written as

$$\zeta_{\rm inflow} = \xi_{\rm outflow} \cdot {\rm SFR} + \kappa. \quad (13)$$

Since the SFR, $M_{\rm gas}$, and κ of progenitor galaxies have been derived in the above sections, given a starting $Z_{\rm gas}(t_0)$ and a set of input parameters (Z_0, y, $\xi_{\rm outflow}$), one can predict the evolution of $Z_{\rm gas}$ at according to Equation (11).

We first assume that the inflow gas is pristine, i.e., $Z_0 = 0$. This is a common assumption taken in most metallicity evolution models. The nucleosynthetic yield, y, is taken as a fixed value depending on the adopted IMF. In the literature, y is around 0.01–0.05 (see Vincenzo et al. 2016, and references therein). The mass loading factor, $\xi_{\rm outflow}$, is dependent on the stellar mass. However, in the mass range considered, i.e., $\log(M_*/M_\odot) = 10.0$–10.7, the dependence of $\xi_{\rm outflow}$ on the mass is quite weak (Peeples & Shankar 2011). We thus assume it to be a constant as well.

With these simplifications, we predict the $Z_{\rm gas}$ evolution of progenitor galaxies at $z < 1.3$, with a time interval of $\Delta t = 0.1$ Gyr. At $z = 1.3$, where the progenitor galaxy has $\log(M_*/M_\odot) = 10.0$, $Z_{\rm gas}$ is $\log({\rm O/H}) + 12 = 8.72$, as predicted by the FMR. In Figure 4, we show three examples of the $Z_{\rm gas}$ evolution curves predicted by our toy model, adopting $y = 0.018$ and three different $\xi_{\rm outflow}$. A nucleosynthetic yield of $y = 0.018$ is chosen because model predictions best match observations near this value, as shown below. As can be seen, the $Z_{\rm gas}$ evolution predicted by our model is quite sensitive to $\xi_{\rm outflow}$.

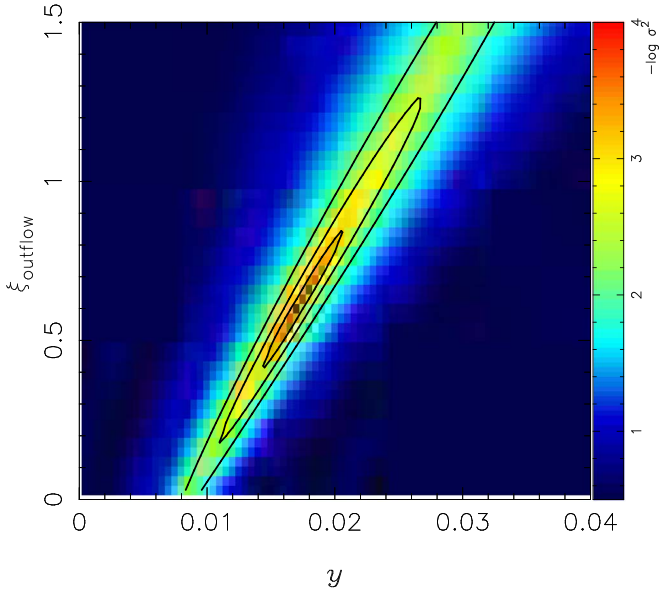

Figure 5. σ^2 map against y and $\xi_{\rm outflow}$. It is clear that the lowest σ^2, i.e., the best matches between model predictions and observations, is found at $\xi_{\rm outflow} \sim 0.5$–$0.8$ and $y \sim 0.015$–0.02.

For a given parameter pair (y, $\xi_{\rm outflow}$), we characterize the degree of the matching between model prediction and observation with

$$\sigma^2 = \sum_{i=1}^{N}\left(\frac{Z_{\rm gas,model}(t_i) - Z_{\rm gas,FMR}(t_i)}{Z_{\rm gas,FMR(t_i)}}\right)^2 / N. \quad (14)$$

In Figure 5, we show the σ^2 map against y and $\xi_{\rm outflow}$. As can be seen, the best-fit mass loading factor is $\xi_{\rm outflow} \sim 0.5$–$0.8$. We insert the median value, $\xi_{\rm outflow} = 0.65$, into Equation (13) to derive the inflow rate $\zeta_{\rm inflow}$. In Figure 6, we show the evolution of $\zeta_{\rm inflow}$ at $z < 1.3$. At first glance, the evolution of $\zeta_{\rm inflow}$ can be largely divided into two phases: a rapidly declining phase at $0.5 < z < 1.3$, and a slowly evolving phase at $z < 0.5$. For comparison, we also plot the evolution of the SFR in Figure 6. At $z > 1.0$, $\zeta_{\rm inflow}$ is clearly higher than the SFR. This may correspond to the "gas accretion epoch" as predicted by theory (Kereš et al. 2005). At $z < 0.5$, the SFR largely mimics the evolution of $\zeta_{\rm inflow}$, suggesting that the $M_{\rm MW}$ progenitor SFGs gradually enter a "quasi-steady" phase at late epochs during which their SFRs are self-regulated by the balance between gas inflows and outflows.

6. Discussion

Combining the observed evolution of the SFR–M_* and $M_{\rm gas}$–M_* relation of SFGs, we constrain the gas flow histories of local Milky Way–mass SFGs since $z = 1.3$. Below, we will compare our results with previous works and discuss the implications of these results.

At $z \sim 1.3$, we find that the net inflow rate κ reaches a level comparable to the SFR (right panel of Figure 3). Papovich et al. (2011) also reported a similar phenomenon for galaxies at a

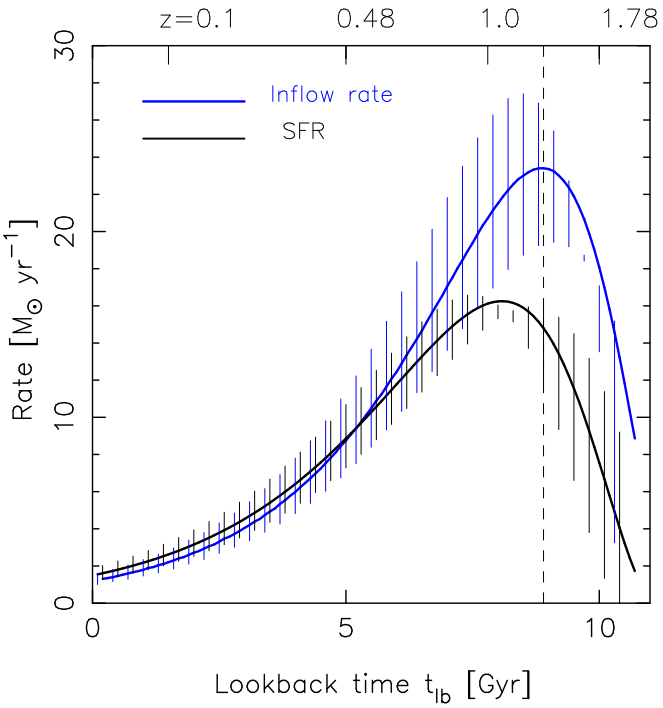

Figure 6. Inferred gas inflow rate $\zeta_{\rm inflow}$ evolution (blue line), applying $\xi_{\rm outflow} = 0.65$. Uncertainties are calculated by including those of the SFR and κ, and ± 0.15 in $\xi_{\rm outflow}$. We also plot the evolution of the SFR for comparison. The dashed line indicates $z = 1.3$.

constant number density of $n = 2 \times 10^{-4}\,{\rm Mpc}^{-3}$ at $z \sim 3.0$ (see their Figure 4). Recently, Scoville et al. (2017) investigated the evolution of κ for SFGs since $z \sim 3.0$. The authors found that the ratio between κ and SFR, κ/SFR, closely correlates with z and M_*:

$$\kappa/{\rm SFR} \sim (1+z)^{0.7}(M_{10}^{0.56} - 0.56 \times M_{10}^{0.74}), \qquad (15)$$

where M_{10} is the stellar mass in units of $10^{10}\,M_\odot$. According to Equation (15), SFGs with $\log(M_*/M_\odot) = 10.0$ typically have $\kappa/{\rm SFR} \sim 0.85$ at $z \sim 1.3$, which is in good agreement with ours.

At $z \sim 0$, we find a very low net inflow rate, $\kappa \sim 0.15 \times$ SFR, for the Milky Way–mass SFGs. This is lower than that reported in Scoville et al. (2017), $\kappa \sim 0.4 \times$ SFR. We emphasize that this discrepancy is largely due to the different treatments on mass-loss rate applied in these two works. From Equation (11) of Scoville et al. (2017), it is clear that the derived κ is directly coupled with the applied return mass fraction R, in the sense that a large R will yield a small κ. In Scoville et al. (2017), the authors used a constant return mass fraction of $R = 0.3$ across $z = 0$–3. In this work, we use the full MSI approach, in which R is not a constant but will increase toward low redshifts, because mass loss contributed from old stellar populations becomes increasingly important at late epochs. At $z \sim 0$, the MSI-based return mass fraction is $R \sim 0.6$, which in turn results in a reduction of $\sim 0.3 \times$ SFR in κ compared to that of Scoville et al. (2017).

We find that the best-fit mass loading factor is $\xi_{\rm outflow} \sim 0.5$–0.8. Although this is quantitatively consistent with that found in some previous works (Lilly et al. 2013; Yabe et al. 2015; Belfiore et al. 2016), it is worthy to note that $\xi_{\rm outflow}$ and y are degenerated in our chemical evolution model, as shown in Figure 5 (also see Peeples & Shankar 2011). As such, the derived $\xi_{\rm outflow}$ is highly sensitive to the choice of y: one must know how many metals are produced before they can determine the level of outflows required to produce the evolution of $Z_{\rm gas}$. To set more stringent constraints on $\xi_{\rm outflow}$, complementary approaches are thus needed.

There appears to be a "turnover" in the gas inflow rate evolution curve at $z \sim 0.5$ (Figure 6). Specifically, at $z = 0.5$–1.3, the change rate of $\zeta_{\rm inflow}$($\frac{d\zeta_{\rm inflow}}{dt}$) is relatively stable with $\frac{d\zeta_{\rm inflow}}{dt} \sim 4.0\,M_\odot\,{\rm Gyr}^{-2}$, whereas at $z < 0.5$, this rate is only $\sim 1.3\,M_\odot\,{\rm Gyr}^{-2}$. What is the physics behind this phenomenon? Under the current framework of galaxy formation, we speculate that this turnover may reveal a switch from the "cold mode" to the "hot mode" accretion near the critical halo mass, $M_{\rm c}$. Interestingly, at the "turnover" redshift, the progenitor galaxies have $\log(M_*/M_\odot) \sim 10.6$, corresponding to a halo mass of $M_{\rm h} \sim 1 \times 10^{12}\,M_\odot$ (Behroozi et al. 2013). This is well consistent with the prediction of the halo-shock heating scenario.

To investigate whether other galaxies also exhibit a similar turnover in $\zeta_{\rm inflow}$ at a same $M_{\rm h}$, we also study SFGs of two different stellar masses (see Figure 9 of the Appendix). For an SFG that with a final stellar mass of $\log(M_*/M_\odot) = 11.0$, we find a similar turnover in its $\zeta_{\rm inflow}$ at $z \sim 0.7$, at which the stellar mass of the progenitor galaxy is around $\log(M_*/M_\odot) = 10.8$. Since these two turnover redshifts are only slightly different, we apply the same $M_{\rm h}$–M_* relation to this galaxy, finding that the corresponding turnover halo mass is $M_{\rm h} \sim 2 \times 10^{12}\,M_\odot$. We argue that the turnover in $\zeta_{\rm inflow}$ does not occur at the same $M_{\rm h}$ for different SFGs. Interestingly, we note that the evolution trend of $M_{\rm turnover}$ is similar to that of $M_{\rm transition}$[5], as reported in Haines et al. (2017, see their Figure 4). This may suggest a connection between the cessation of star formation in galaxies and the significant change in their gas inflow behaviors, as we will argue below.

Although this work is focused on the gas flow behavior of SFGs, our results may provide some insights in interpreting the star formation quenching of galaxies near or above M^* ("mass quenching"; see Peng et al. 2010). Since the tight SFR–M_* relation exists up to at least $z \sim 5$–6 (Speagle et al. 2014; Tasca et al. 2015), the progenitors of massive quenched galaxies are expected to be normal SFGs before they get quenched. As such, a quenched galaxy should also experience a "rapidly declining phase" in $\zeta_{\rm inflow}$ during a certain epoch. When $\zeta_{\rm inflow}$ has significantly decreased, the impact of internal processes on galaxy evolution will become increasingly important. It has been suggested that violent bulge build-up processes are often accompanied with gas outflow driven by strong starburst or AGN activities (or both), which is expected to be capable in cleaning the gas reservoir in a relatively short timescale (Hopkins et al. 2006; Geach et al. 2014, 2018). Since $\zeta_{\rm inflow}$ has significantly decreased and the gas replenishment timescale is long, the removal of gas reservoir may drive the galaxy to rapidly get quenched. Observationally, rapidly quenching systems (known as "post-starburst" galaxies) are found to be bulge-dominated with a surprisingly high AGN fraction, supporting this scenario (Vergani et al. 2010; Yesuf et al. 2014; Baron et al. 2018). On the other hand, bar-driven bulge build-up processes may also play an important role in

[5] $M_{\rm transition}$ is the stellar mass at which the fraction of quenched galaxies reaches $f_{\rm quenched} = 50\%$.

exhausting the cold gas reservoirs, although the timescale is relatively long (Masters et al. 2012; Wang et al. 2012; Cheung et al. 2013; Gavazzi et al. 2015; Lin et al. 2017).

When a prominent bulge has been formed, other internal processes may also play a role in further suppressing star formation. Using cosmological simulations, Martig et al. (2009) illustrated that a prominent bulge is able to stabilize the gas disk against fragmentation to form stars. Recently, such kinds of dynamically driven star formation suppression are reported in observational studies (Davis et al. 2014; Genzel et al. 2014b). In addition, a bulge will play a role in preventing the the cooling of recycled gas. This is because, in dispersion-supported (spheroidal) systems, a considerable fraction of the recycled gas will quickly mix with halo gas (Parriott & Bregman 2008). By contrast, in disk-dominated galaxies, the recycled gas can directly return to the corotating interstellar medium to form next-generation stars. Finally, winds driven by low-level AGNs appear capable in heating the surrounding gas to prevent star formation at the late epochs of galaxy evolution (Cheung et al. 2016; Weinberger et al. 2017, 2018; Li et al. 2018). In summary, we suggest that a significant decline in gas inflow rate is the first step required to quench a massive galaxy. Once this happens, bulge-related internal processes likely play an important role in quenching star formation, resulting in the strong correlation between the specific SFR and surface mass density (Bell 2008; Franx et al. 2008; Bell et al. 2012; Cheung et al. 2012; Fang et al. 2013; Barro et al. 2017; Whitaker et al. 2017).

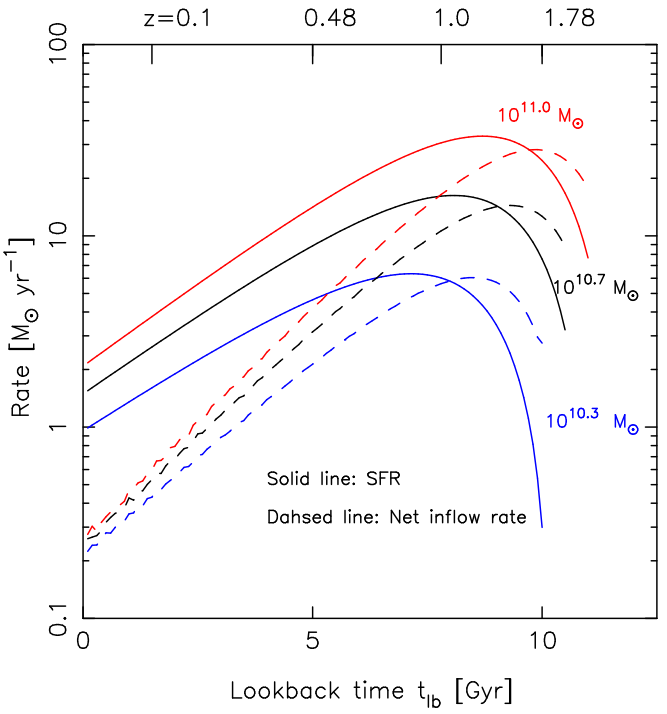

Figure 7. SFR and the net inflow rate as a function of cosmic time for galaxies with different masses. SFRs and net inflow rates are indicated in solid lines and dashed lines, respectively. Galaxies of different masses are indicated in different colors.

7. Summary and Conclusions

In this paper, we study the gas flow histories for the progenitors of local Milky Way–mass star-forming galaxies out to $z \sim 1.3$. Assuming that the progenitor galaxies grow in their stellar mass mainly via star formation (not via mergers), then their stellar mass growth histories can be traced following the evolution of the SFR–M_* relation. Using the molecular gas-scaling relations established by Tacconi et al. (2018), we derive the molecular gas mass of progenitor galaxies. The H I gas mass is estimated based on the $M_{\rm H\,I}$–M_* relation established at $z = 0$, assuming that this relation does not evolve out to $z = 1.3$. With the $M_* + M_{\rm gas}$ growth curve and chemical evolution modeling of progenitor galaxies, we have found the following:

1. From $z = 1.3$ to $z = 0$, the net inflow rate κ decreases by a factor of $\sim \times 50$, whereas the SFR decreases $\sim \times 10$. At $z = 0$, κ is only $\sim$0.15 $\times$ SFR.
2. The mean outflow rate is $\sim$(0.5–0.8) $\times$ SFR.
3. The inflow rate, $\zeta_{\rm inflow}$, experiences a "rapidly declining phase" at $z = 0.5$–1.3, during which $\zeta_{\rm inflow}$ decreases by $\sim$80%. At $z < 0.5$, $\zeta_{\rm inflow}$ continuously decreases but with a much lower decreasing rate.

We suggest that when the gas inflow rate has significantly decreased, bulge-related internal processes likely play an important role in quenching star formation.

We thank the anonymous referee for constructive suggestions that help to improve the clarity of the manuscript. This work was partially supported by the National Key Research and Development Program ("973" program) of China (No. 2015CB857004, 2016YFA0400702, 2017YFA0402600, and 2017YFA0402703), the National Natural Science Foundation of China (NSFC, Nos. 11773001, 11721303, 11703092, 11320101002, 11421303, 11433005, 11773076, and 11721303), and the Natural Science Foundation of Jiangsu Province (No. BK20161097).

Appendix

For comparison, we have also studied the gas inflow and outflow histories of SFGs with final stellar masses lower or higher than $M_{\rm MW}$. Here, we present the results of two SFGs: one with a final stellar mass of log $(M_*/M_\odot) = 10.3$ and the other with log $(M_*/M_\odot) = 11.0$. For the low-mass SFG, the application of our methodology should be safe. For the high-mass one, we assume that the growth of its stellar mass is also dominated by in situ star formation (not by mergers), and our method is still valid. This is supported by the study of Moster et al. (2013), who found that mergers only contribute <20% to the total stellar mass budget of a log $(M_{\rm h}/M_\odot) = 13.0$ halo.

The stellar mass growth histories and gas masses of these two galaxies are derived using the method described in Sections 2 and 3. In Figure 7, we compare the star formation, as well as the net gas inflow histories of these two SFGs, with those of the $M_{\rm MW}$ SFG. As can be seen, the star formation of high-mass SFGs peaks at higher redshifts than that of the low-mass ones. Another interesting feature is that the decreasing rate of the net inflow rate is also mass dependent, where the most massive SFG has the highest net inflow decreasing rate.

We then model the $Z_{\rm gas}$ evolution of these two galaxies with the same method described in Section 5. The beginning redshifts are selected at which the galaxy has log $(M_*/M_\odot) = 10.0$. These correspond to $z = 0.7$ and $z = 1.9$ for the low-mass and high-mass SFG, respectively. In Figure 8, we present the σ map against y and $\xi_{\rm outflow}$. As shown in the top

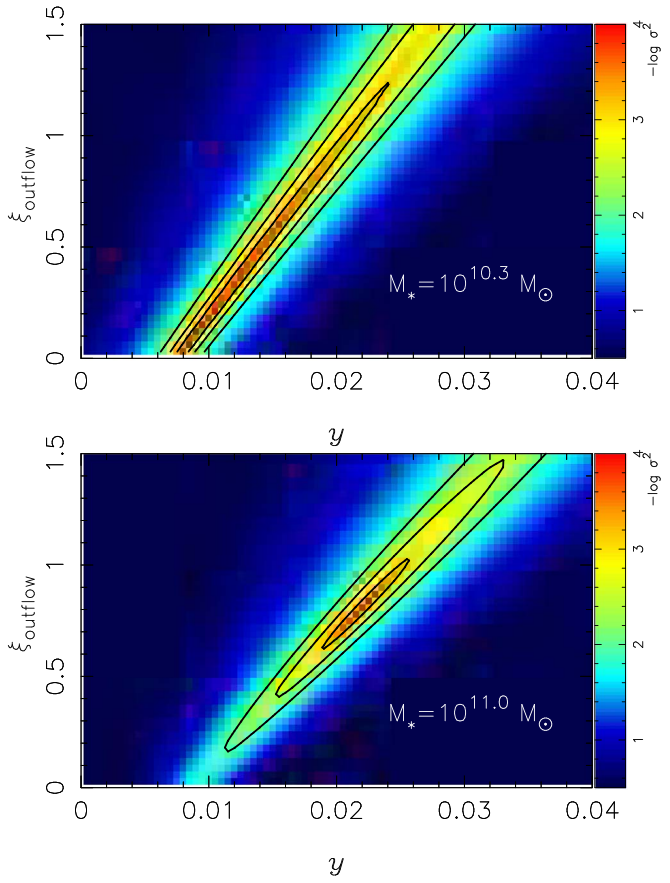

Figure 8. Similar to Figure 5 but for SFGs with log $(M_*/M_\odot) = 10.3$ and log $(M_*/M_\odot) = 11.0$.

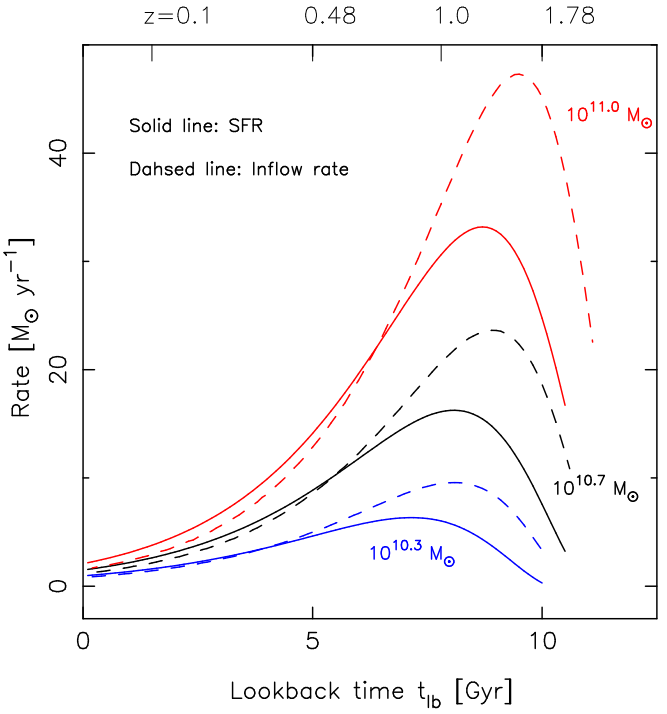

Figure 9. Similar to Figure 6 but for SFGs with three different masses.

panel, y and $\xi_{outflow}$ cannot be very well constrained for the low-mass galaxy, which is mainly due to the narrow redshift range available for the fitting procedure. For the high-mass galaxy, y and $\xi_{outflow}$ are better constrained, with the best fit of $y \sim 0.023$ and $\xi_{outflow} \sim 0.8$. Note that both y and $\xi_{outflow}$ are slightly higher than those derived for the M_{MW} SFG.

A comparison between Figures 5 and 8 indicates that $\xi_{outflow}$ may be mass-dependent. This conflicts with our model assumption that $\xi_{outflow}$ is largely independent on stellar mass at log $(M_*/M_\odot) > 10.0$. We consider that this confliction may arise from the following aspects. First, the mass independence of $\xi_{outflow}$ at log $(M_*/M_\odot) > 10.0$ is derived from the modeling of the mass–metallicity relation of low-redshift SFGs (Spitoni et al. 2010; Peeples & Shankar 2011). For a certain SFG, it is difficult to determine whether $\xi_{outflow}$ is roughly a constant during its evolution at log $(M_*/M_\odot) > 10.0$, because the $\xi_{outflow}$–M_* relation may have evolved from high-z to low-z. Second, the uncertainties of all input parameters, such as M_{gas}, κ, and SFR, will more or less contribute to the output of $\xi_{outflow}$. Finally, the scatter of the FMR, which is at a level of $\Delta\log(O/H) \sim 0.05$ dex (Mannucci et al. 2010), is not taken into account during the fitting procedure. The combination of these factors may result in an offset between the output $\xi_{outflow}$ and the true value. It is thus important to access whether the output $\xi_{outflow}$ is reliable. When the same $y = 0.018$ is adopted, the best-fit mass loading factor is $\xi_{outflow} = 0.8$ and 0.5 for the low-mass and high-mass SFGs, respectively. To our knowledge, the difference between these two values is not significant, and we think that our initial model assumption (i.e., $\xi_{outflow}$ = constant) is still valid. Fixing $y = 0.018$, we have also tried to use a mass-dependent $\xi_{outflow}$, which is parameterized by $\xi_{outflow} = a + b \times [\log(M_*/M_\odot) - 10.0]$ to set a constraint on $\xi_{outflow}$. We investigated the σ map against a and b and found that the best match is always near $b \sim -0.1$, i.e., $\xi_{outflow}$ is indeed very weakly dependent on M_* at log $(M_*/M_\odot) > 10.0$. In the following section, we still assume that $\xi_{outflow}$ is a constant across the mass range of log $(M_*/M_\odot) = [10.0, 11.0]$ and adopt a median value of $\xi_{outflow} = 0.65$.

In Figure 9, we show the evolution of the SFR and the inflow rate for the three galaxies shown in Figure 7, adopting $\xi_{outflow} = 0.65$. As can be seen, the inflow rates of these galaxies all exceed the SFRs in their early assembly epochs, and the inflow rates reach the peak values earlier than the SFRs by ~1 Gyr. Similar to Figure 6, we define the epoch at which SFR = ζ_{inflow} as the "turnover" redshift. As can be seen, the turnover redshift is ~0.7 for the most massive SFG, at which the progenitor galaxy has log $(M_*/M_\odot) \sim 10.8$. At $z < z_{turnover}$, the behaviors of ζ_{inflow} are very close to the SFRs for all three SFGs.

ORCID iDs

Zhizheng Pan https://orcid.org/0000-0001-5662-8217
Xianzhong Zheng https://orcid.org/0000-0003-3728-9912
Xu Kong https://orcid.org/0000-0002-7660-2273

References

Baron, D., Netzer, H., Prochaska, J. X., et al. 2018, MNRAS, 480, 3993
Barro, G., Faber, S. M., Koo, D. C., et al. 2017, ApJ, 840, 47
Behroozi, P., Wechsler, R., Hearin, A., & Conroy, C. 2018, arXiv:1806.07893
Behroozi, P. S., Wechsler, R. H., & Conroy, C. 2013, ApJ, 770, 57
Belfiore, F., Maiolino, R., & Bothwell, M. 2016, MNRAS, 455, 1218
Bell, E. F. 2008, ApJ, 682, 355
Bell, E. F., van der Wel, A., Papovich, C., et al. 2012, ApJ, 753, 167
Bouché, N., Dekel, A., Genzel, R., et al. 2010, ApJ, 718, 1001

Catinella, B., Schiminovich, D., Cortese, L., et al. 2013, MNRAS, 436, 34
Catinella, B., Schiminovich, D., Kauffmann, G., et al. 2010, MNRAS, 403, 683
Chabrier, G. 2003, PASP, 115, 763
Cheung, E., Athanassoula, E., Masters, K. L., et al. 2013, ApJ, 779, 162
Cheung, E., Bundy, K., Cappellari, M., et al. 2016, Natur, 533, 504
Cheung, E, Faber, S., Koo, D., et al. 2012, ApJ, 760, 131
Cicone, C., Maiolino, R., & Marconi, A. 2016, A&A, 588, A41
Cicone, C., Maiolino, R., Sturm, E., et al. 2014, A&A, 562, A21
Combes, F., García-Burillo, S., Braine, J., et al. 2011, A&A, 528, A124
Cresci, G., Mannucci, F., Sommariva, V., et al. 2012, MNRAS, 421, 262
Daddi, E., Bournaud, F., Walter, F., et al. 2010, ApJ, 713, 686
Davé, R., Finlator, K., & Oppenheimer, B. D. 2011, MNRAS, 416, 1354
Davé, R., Finlator, K., & Oppenheimer, B. D. 2012, MNRAS, 421, 98
Davis, T. A., Young, L. M., Crocker, A. F., et al. 2014, MNRAS, 444, 3427
Dekel, A., & Birnboim, Y. 2006, MNRAS, 368, 2
Dekel, A., Birnboim, Y., Engel, G., et al. 2009a, Natur, 457, 451
Dekel, A., Sari, R., & Ceverino, D. 2009b, ApJ, 703, 785
Fang, J. J., Faber, S. M., Koo, D. C., & Dekel, A. 2013, ApJ, 776, 63
Finlator, K., & Davé, R. 2008, MNRAS, 385, 2181
Franx, M., van Dokkum, P. G., Förster Schreiber, N. M., et al. 2008, ApJ, 688, 770
Gavazzi, G., Consolandi, G., Dotti, M., et al. 2015, A&A, 580, A116
Geach, J. E., Hickox, R. C., Diamond-Stanic, A. M., et al. 2014, Natur, 516, 68
Geach, J. E., Tremonti, C., Diamond-Stanic, A. M., et al. 2018, ApJL, 864, L1
Genzel, R., Förster Schreiber, N. M., Lang, P., et al. 2014a, ApJ, 765, 7
Genzel, R., Förster Schreiber, N. M., Lang, P., et al. 2014b, ApJ, 785, 75
Genzel, R., Tacconi, L. J., Lutz, D., et al. 2015, ApJ, 800, 20
Giovanelli, R., Haynes, M. P., Kent, B. R., et al. 2005, AJ, 130, 2598
Haines, C. P., Iovino, A., Krywult, J., et al. 2017, A&A, 605, A4
Haywood, M., Lehnert, M. D., Di Matteo, P., et al. 2016, A&A, 589, A66
Heckman, T. M., Armus, L., & Miley, G. K. 1990, ApJS, 74, 833
Henry, A., Scarlata, C., Domínguez, A., et al. 2013, ApJL, 776, L27
Hopkins, P. F., Hernquist, L., Cox, T. J., et al. 2006, ApJS, 163, 1
Hopkins, P. F., Quataert, E., & Murray, N. 2012, MNRAS, 421, 3522
Huang, S., Haynes, M. P., Giovanelli, R., & Brinchmann, J. 2012, ApJ, 756, 113
Kereš, D., Katz, N., Weinberg, D. H., & Davé, R. 2005, MNRAS, 363, 2
Larson, R. B., Tinsley, B. M., & Caldwell, C. N. 1980, ApJ, 237, 692
Lee, N., Sanders, D. B., Casey, C. M., et al. 2015, ApJ, 801, 80
Leitner, S. N., & Kravtsov, A. V. 2011, ApJ, 734, 48
Li, Y.-P., Yuan, F., Mo, H., et al. 2018, ApJ, 866, 70
Lilly, S. J., Carollo, C. M., Pipino, A., Renzini, A., & Peng, Y. 2013, ApJ, 772, 119
Lin, L., Li, C., He, Y., Xiao, T., & Wang, E. 2017, ApJ, 838, 105
Maier, C., Lilly, S. J., Ziegler, B. L., et al. 2014, ApJ, 792, 3
Maiolino, R., Nagao, T., Grazian, A., et al. 2008, A&A, 488, 463
Mannucci, F., Cresci, G., Maiolino, R., Marconi, A., & Gnerucci, A. 2010, MNRAS, 408, 2115
Martig, M., Bournaud, F., Teyssier, R., & Dekel, A. 2009, ApJ, 707, 250
Masters, K. L., Nichol, R. C., Haynes, M. P., et al. 2012, MNRAS, 424, 2180
McMillan, P. J. 2017, MNRAS, 465, 76
Moster, B. P., Naab, T., & White, S. D. M. 2013, MNRAS, 428, 3121
Papovich, C., Finkelstein, S. L., Ferguson, H. C., Lotz, J. M., & Giavalisco, M. 2011, MNRAS, 412, 1123
Papovich, C., Labbé, I., Quadri, R., et al. 2015, ApJ, 803, 26
Parriott, J. R., & Bregman, J. N. 2008, ApJ, 681, 1215
Patel, S. G., Fumagalli, M., Franx, M., et al. 2013, ApJ, 778, 115
Peeples, M. S., & Shankar, F. 2011, MNRAS, 417, 2962
Peng, Y.-j., Lilly, S. J., Kovač, K., et al. 2010, ApJ, 721, 193
Peng, Y.-j., & Maiolino, R. 2014, MNRAS, 443, 3643
Popping, G., Caputi, K. I., Trager, S. C., et al. 2015, MNRAS, 454, 2258
Qu, Y., Helly, J. C., Bower, R. G., et al. 2017, MNRAS, 464, 1659
Rémy-Ruyer, A., Madden, S. C., Galliano, F., et al. 2014, A&A, 563, A31
Rubin, K. H. R., Prochaska, J. X., Koo, D. C., et al. 2014, ApJ, 794, 156
Saintonge, A., Catinella, B., Tacconi, L. J., et al. 2017, ApJS, 233, 22
Saintonge, A., Kauffmann, G., Kramer, C., et al. 2011, MNRAS, 415, 32
Salim, S., Lee, J. C., Davé, R., & Dickinson, M. 2015, ApJ, 808, 25
Sanders, R. L., Shapley, A. E., Kriek, M., et al. 2015, ApJ, 799, 138
Sanders, R. L., Shapley, A. E., Kriek, M., et al. 2018, ApJ, 858, 99
Sato, T., Martin, C. L., Noeske, K. G., Koo, D. C., & Lotz, J. M. 2009, ApJ, 696, 214
Schreiber, C., Pannella, M., Elbaz, D., et al. 2015, A&A, 575, A74
Scoville, N., Lee, N., Vanden Bout, P., et al. 2017, ApJ, 837, 150
Speagle, J. S., Steinhardt, C. L., Capak, P. L., & Silverman, J. D. 2014, ApJS, 214, 15
Spitoni, E., Calura, F., Matteucci, F., & Recchi, S. 2010, A&A, 514, A73
Spitoni, E., Vincenzo, F., & Matteucci, F. 2017, A&A, 599, A6
Stewart, K. R., Kaufmann, T., Bullock, J. S., et al. 2011, ApJL, 735, L1
Tacconi, L. J., Genzel, R., Neri, R., et al. 2010, Natur, 463, 781
Tacconi, L. J., Genzel, R., Saintonge, A., et al. 2018, ApJ, 853, 179
Tacconi, L. J., Neri, R., Genzel, R., et al. 2013, ApJ, 768, 74
Tasca, L. A. M., Le Fèvre, O., Hathi, N. P., et al. 2015, A&A, 581, A54
Tomczak, A. R., Quadri, R. F., Tran, K.-V. H., et al. 2016, ApJ, 817, 118
van de Voort, F., Schaye, J., Booth, C. M., Haas, M. R., & Dalla Vecchia, C. 2011, MNRAS, 414, 2458
van Dokkum, P. G., Leja, J., Nelson, E. J., et al. 2013, ApJL, 771, L35
Vergani, D., Zamorani, G., Lilly, S., et al. 2010, A&A, 509, A42
Vincenzo, F., Matteucci, F., Belfiore, F., & Maiolino, R. 2016, MNRAS, 455, 4183
Wang, J., Kauffmann, G., Overzier, R., et al. 2012, MNRAS, 423, 3486
Weinberger, R., Springel, V., Hernquist, L., et al. 2017, MNRAS, 465, 3291
Weinberger, R., Springel, V., Pakmor, R., et al. 2018, MNRAS, 479, 4056
Weiner, B. J., Coil, A. L., Prochaska, J. X., et al. 2009, ApJ, 692, 187
Whitaker, K. E., Bezanson, R., van Dokkum, P. G., et al. 2017, ApJ, 838, 19
Whitaker, K. E., Franx, M., Leja, J., et al. 2014, ApJ, 795, 104
Wolfire, M. G., McKee, C. F., Hollenbach, D., & Tielens, A. G. G. M. 2003, ApJ, 587, 278
Yabe, K., Ohta, K., Akiyama, M., et al. 2015, ApJ, 798, 45
Yabe, K., Ohta, K., Iwamuro, F., et al. 2014, MNRAS, 437, 3647
Yesuf, H. M., Faber, S. M., Trump, J. R., et al. 2014, ApJ, 792, 84
Zahid, H. J., Dima, G. I., Kudritzki, R.-P., et al. 2014, ApJ, 791, 130
Zahid, H. J., Geller, M. J., Kewley, L. J., et al. 2013, ApJL, 771, L19